Microwave Bistability in a Magnetostatic Wave Interferometer with External Feedback

Yuri K. Fetisov, *Senior Member, IEEE*, and Carl E. Patton, *Fellow, IEEE*

***Abstract*— Microwave bistability has been obtained for the first time in a magnetostatic wave (MSW) interferometer with external magnetic field feedback. The interferometer contained a magnetostatic surface wave transmission line with a 7.5-μm-thick epitaxial film of yttrium iron garnet magnetized with an external static magnetic field of 1048 Oe, a variable attenuator in a parallel reference channel, and external feedback in the form of an additional static field derived from the line output. Bistable and multistable output power versus input power responses are derived from the frequency dependence of the interferometer transmission and the MSW wave number dependence on the static magnetic field. Typical bistable and multistable output versus input power hysteresis loops were obtained under constant frequency operation in the range 4.9 to 5.2 GHz, and for input powers from -30 to $+10$ dBm. The bistable response depends on the frequency of the microwave signal, the attenuation in the reference channel, and the gain of the feedback loop. An analysis based on linear MSW theory agreed with experiment. Applications of MSW microwave bistability include power limiter devices and basic microwave logic elements.**

***Index Terms*— Bistable circuits, ferrite devices, ferrite films, magnetic microwave devices, magnetic resonance.**

I. Introduction

THE characteristics of magnetostatic wave (MSW) excitations in yttrium iron garnet (YIG) films depend on the size and orientation of the external static magnetic field. The MSW frequency band may be tuned over a range of 1–20 GHz and the excitation wave number and group velocity may be changed by an order of magnitude or more simply by changing the magnetic field by tens of Oe. This controllability of MSW properties as well as the relatively low microwave loss in YIG provide a unique opportunity for the investigation of wave phenomena which are difficult to observe for acoustic or optical waves in solids.

Many effects have been observed in MSW structures due to magnetic field modulation during launch or propagation of these waves in YIG film devices [1]. These include the dynamic compression of wave packets, the parametric interaction of MSW signals of different frequencies and different wave numbers, and synchronization of the modes to form short microwave pulses, among others. These effects have also been used to advantage in the design of microwave signal processing devices [2].

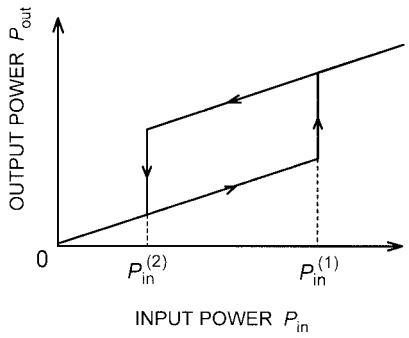

Fig. 1. Characteristic output power $P_{\rm out}$ versus input power $P_{\rm in}$ response for a bistable system. Bistable behavior occurs for input powers in the range $P_{\rm in}^{(2)} < P_{\rm in} < P_{\rm in}^{(1)}$.

The objective of this work was to investigate a new effect in MSW systems, bistable, and multistable behavior produced by feedback. The basic transmission characteristic of a bistable system is shown in Fig. 1. The output power $P_{\rm out}$ is a multivalued function of the input power $P_{\rm in}$. As the input power increases from zero, $P_{\rm out}$ increases smoothly and then experiences an abrupt jump to higher values at $P_{\rm in} = P_{\rm in}^{(1)}$. If the input power is decreased from some value above $P_{\rm in}^{(1)}$, one follows the upper branch of the response down to an input power at $P_{\rm in} = P_{\rm in}^{(2)}$ and then $P_{\rm out}$ jumps back to the lower branch.

As shown in [3] for optical systems, two conditions must be satisfied for bistability to exist in a wave based system. First, the transmission or reflection coefficient of the system must have some characteristic dependence on the frequency or wave number of the excitation. Second, some sort of feedback must exist which can change some characteristic of the signal, such as the wave number or damping coefficient, as a function of the transmitted or reflected power. One has a dispersive type bistability when the carrier wave number is controlled through the feedback. One has an absorptive bistability when the damping is the feedback parameter. One may have other types of bistability as well. One has a so-called intrinsic type bistability when the wave characteristics depend directly on the power, as for nonlinear excitations. One can have a hybrid type bistability when the wave characteristics are changed through

Manuscript received May 13, 1998; revised June 11, 1998. This work was sponsored in part by the National Science Foundation under Grants DMR-9400276 and DMR-9801649 and by the U.S. Army Research Office under Grants DAAH04-95-1-0325 and DAAG55-98-1-0430.

Y. K. Fetisov is with the Department of Physics, Colorado State University, Fort Collins, CO 80523 USA, on leave from the Moscow Institute of Radio Engineering, Electronics, and Automation, Moscow, Russia.

C. E. Patton is with the Department of Physics, Colorado State University, Fort Collins, CO 80523 USA.

Publisher Item Identifier S 0018-9464(99)02012-9.

some other control parameter which, in turn, depends on the power.

This report describes a hybrid dispersive multistable system based on magnetostatic waves in a YIG film. The variation in output power with wave number derives from an interferometer arrangement with the MSW element in parallel with a second reference line. Feedback is applied in the form of a static magnetic field which is controlled by the output power from the interferometer circuit. This type of bistable MSW device, for which the system parameters can be easily controlled over a wide range, is of interest for microwave applications. It also provides a convenient arrangement for a first investigation of bistable and multistable processes in YIG film microwave devices.

Theoretical issues related to intrinsic dispersive MSW bistability in periodic structures are discussed in [4]. There has also been a recently observed absorptive bistability in MSW oscillators [5]. These topics are outside the scope of the present work.

Section II describes the MSW interferometer with the magnetic field feedback and the experimental set up for the measurements.

Section III-A presents the measured frequency response and dispersion characteristic for the MSW transmission line taken by itself and for the entire interferometer, but without feedback. Section III-B describes the effect of the external feedback on the interferometer frequency response as a function of the input microwave power level. Section III-C then gives representative bistability response curves for the device for different signal input frequencies, different interferometer conditions, and different levels of feedback. Some peculiarities of pulsed operation of the bistable MSW interferometer are considered in Section III-D.

Section IV-A gives a qualitative explanation of the bistability mechanism for the MSW interferometer and describes a method for calculation of bistability response curves. Section IV-B then presents some representative results from numerical simulations. These results illustrate possibilities for the control of the transmission characteristics of a bistable MSW interferometer and provide a comparison with experiment. Section VI-C provides basic working equations for the analytical understanding of the bistable response.

II. Bistable Interferometer System

A diagram of the MSW interferometer, the feedback arrangement, and the microwave measurement system is shown in Fig. 2. The interferometer consists of the two parallel arms in the center of the diagram, with the magnetostatic surface wave (MSSW) YIG film device in the upper arm and the variable attenuator with attenuation A in the lower arm. The MSSW structure is described below. The labels H and L refer to the total magnetic field applied to the MSSW device and the MSSW line power transmission coefficient, respectively. Both parameters will be important for the analysis below.

The interferometer is driven by the microwave source on the left side of the diagram through the power divider D. The output from the interferometer is obtained from the power

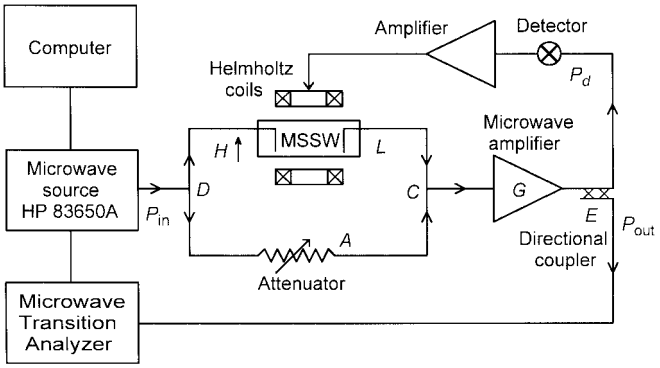

Fig. 2. Block diagram of the MSW interferometer, feedback, and microwave measurement systems. The interferometer contains a MSSW transmission line in the upper arm and a variable attenuator A in the lower arm, with an input power divider D and output power combiner C. The feedback loop consists of a microwave amplifier of gain G, directional coupler E, the microwave diode detector, the dc current amplifier, and the pair of Helmholtz coils. Data are obtained through the microwave transition analyzer and the computer. The parameters H and L indicate the total magnetic field applied to the MSSW line and the transmission coefficient of the line, respectively.

combiner C and applied to a microwave amplifier of gain G. Part of this output signal is then routed to a diode detector and a dc current amplifier. This amplifier drives a pair of Helmholtz coils to provide magnetic field feedback to the MSSW device. Part of the output signal is picked off from the directional coupler E and routed to the microwave transition analyzer for data analysis.

The three important power points are noted in Fig. 2. The input power $P_{\rm in}$ is measured at the input to power divider D. The output power $P_{\rm out}$ is measured at the takeoff from the directional coupler E. The microwave power at the detector is noted as P_d.

The MSSW transmission line is of standard design and has been described elsewhere [6]. The line contains a long and narrow 2 mm by 20 mm rectangular YIG film of thickness 7.5 μm. The film was grown by standard liquid-phase-epitaxy methods on a gallium-gadolinium-garnet substrate of thickness 0.5 mm. The film was provided by Dr. J. D. Adam of the Northrop Grumman Research and Development Laboratories, Pittsburgh, Pennsylvania. The film had a nominal YIG saturation induction of 1750 G and a 9.3 GHz half power ferromagnetic resonance line width of 0.98 Oe, measured with the static magnetic field in plane. For the purposes of this paper, all magnetic parameters will be expressed in Gaussian units.

The MSSW transmission line circuit consists of two microstrip transducers of 50 μm width and 3 mm length deposited on the surface of a 0.5 mm thick alumina substrate at a distance $\Lambda = 6$ mm apart from each other. The YIG film was placed across and in close contact with these elements. The entire structure was placed in a uniform static external magnetic field $H_S = 1048$ Oe, applied in the film plane and perpendicular to the long film axis and the MSSW propagation direction. The Helmholtz coil pair was positioned to provide an additional feedback magnetic field H_F parallel to the static field H_S.

The interferometer response is controlled by the delay and attenuation for the MSSW signal in the upper arm and the

level of attenuation in the lower arm of the interferometer in Fig. 2. The variable attenuator provided an attenuation A from 0 dB to -18 dB. The interference condition between the MSSW signal and the reference signal in the lower arm will be critical to the bistable response.

Turn now to the feedback elements. The microwave amplifier at the output of the interferometer is a monolithic GaAs amplifier with a frequency bandwidth of 2–8 GHz, a low power gain coefficient $G = 34$ dB at 5 GHz, and a maximum output power level of 1 W. The external feedback loop in Fig. 2 contains the directional coupler E with a coupling coefficient $B = -20$ dB and forward insertion loss of 0.5 dB, a microwave diode, a dc current amplifier with a maximum output current of 0.4 A, and the Helmholtz coil pair. This coil had a resistance of 40.7 Ω. Referenced to the microwave power at the diode input P_d, this arrangement provided a nearly linear response for the magnetic field H_F. The field response $\Delta H_F/\Delta P_d$ was 1.9 Oe/mW for power levels up to $P_d = 40$ mW.

A Hewlett Packard model 83 650A synthesized sweeper was used as a source for continuous wave (CW) microwave power in the 4–6 GHz frequency band and at power levels up to 20 dBm. A Hewlett Packard model 70 820A microwave transition analyzer was used to measure the frequency response, phase response, and power response of the various components of the system, and for time domain measurements of the various characteristics of the microwave pulses. All data were collected and analyzed through a personal computer.

III. Experimental Results

A. CW Characteristics of the MSSW Interferometer

Fig. 3 shows typical measured and calculated values of the power transmission coefficient L and wave number k versus frequency f for the MSSW transmission line taken alone. The measurements were carried out with an input microwave power level of -10 dBm and a frequency sweep time of 30 s. The static magnetic field was 1048 Oe. The dependence of the MSSW wave number on frequency was found from the measured phase response of the line.

The theoretical curves were obtained from basic MSSW theory for isotropic films [7] and for an adjusted static magnetic field value of 1067 Oe. This adjustment was needed to position the calculated MSSW frequency band over the same range as the data. The discrepancy between this magnetic field and the experimental field is due to demagnetizing effects and anisotropy.

The calculated transmission coefficient results in Fig. 3(a) were obtained as described in [8]. The various dimensions of the transmission line structure, the magnetic parameters cited above, the nonuniform distribution of microwave currents across and along the strip line transducers, impedance matching conditions, and the MSSW magnetic propagation losses were all taken into account. The magnetic loss was based on a measured ferromagnetic resonance half power linewidth of 0.98 Oe at 9.3 GHz, taken to scale linearly with frequency.

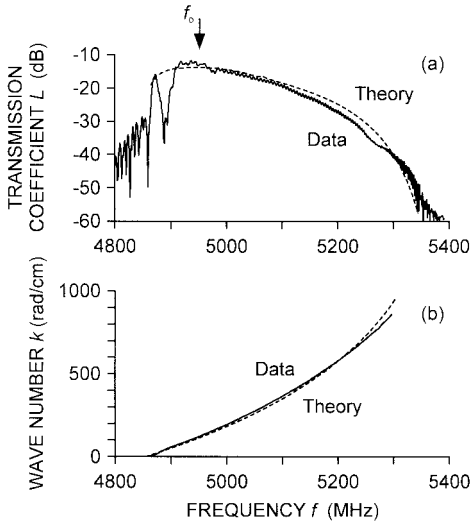

Fig. 3. (a) Power transmission coefficient L versus frequency f and (b) wave number k versus frequency f for the MSSW transmission line described in the text. The solid lines show experimental data and the dashed lines show calculated responses as described in the text. The f_o point at 4950 MHz is near the maximum of the transmission.

The calculated curve for MSSW wave number k versus frequency f was obtained from the dispersion equation for magnetostatic surface waves in a ferrite film of infinite extent, after the work of Damon and Eshbach [7]. The Damon and Eshbach MSSW dispersion relation may be written in the form

$$k = \frac{1}{2d} \ln\left\{ \frac{f_M^2}{4[(f_H + f_M/2)^2 - f^2]} \right\}. \tag{1}$$

The parameter d denotes the film thickness. The frequency parameter f_H expresses the static field in frequency units according to $f_H = |\gamma|H$, where $|\gamma| = 2.8$ MHz/Oe is the absolute value of the gyromagnetic ratio. The frequency parameter f_M expresses the ferrite saturation induction $4\pi M$ in frequency units as well, according to $f_M = |\gamma|4\pi M$. Note that (1) yields a low frequency band edge at $k = 0$, denoted by f_B, given by

$$f_B = \sqrt{f_H(f_H + f_M)}. \tag{2}$$

This band edge is seen to change with the static field H_S applied to the device.

Fig. 3(a) shows that for the given operating parameters, MSSW signal transmission was supported over a frequency band from about 4850 MHz to 5400 MHz. This band is well above the frequency region where nonlinear saturation of the wave power could take place [9]. The frequency point for minimum loss was at about 4.95 GHz. The transmission coefficient at this frequency was -12.7 dB. This frequency will be denoted as f_o and taken as the nominal operating frequency for many of the results to be considered shortly. This operating point is indicated by the arrow labeled f_o in Fig. 3(a).

The transmission response in Fig. 3(a) also shows a distinct notch near the low frequency edge of the band. This notch is due to a distortion of the MSSW dispersion characteristic because of the metallization on the back side of the alumina substrate [10]. This effect is not critical for the present work.

This interaction was ignored in the calculations described above and shown in Fig. 3.

Note from Fig. 3(b) that over the frequency band for appreciable MSSW signal transmission, the MSSW wave number moves from zero at the low frequency edge of the band up to k values in excess of 800 rad/cm at the top of the band. This variation in wave number with frequency at fixed field, or conversely, with field at fixed frequency, provides a phase change in the MSSW transmission line output signal. This phase change, in combination with the reference signal from the bottom arm of the interferometer, leads to an interference at the output. This response, in turn, will be used to produce the desired bistability.

From the results in Fig. 3, one can see that the basic surface wave theory can account quite well for the characteristics of the MSSW transmission line taken alone. The shape of the measured frequency response and the dispersion were not affected by increases in the line input power level up to 10 dBm. This power limit of 10 dBm will be taken as an upper limit for a linear MSSW response for the line.

Fig. 4 shows corresponding response curves for combined signals from the MSSW arm and the lower reference arm of the interferometer in Fig. 2, but still without feedback. Fig. 4(a) shows the results of measurements and Fig. 4(b) shows modeling results which were obtained under the same assumptions and approximations as used for the Fig. 3 calculations. Details of the modeling will be considered below. For the data of Fig. 4(a), the input power to the interferometer was set at 1 mW and the attenuator setting A for the lower arm was -14 dB. The MSSW line parameters were the same as for Fig. 3.

The results in Fig. 4 show that the interference of the MSSW signal and the reference microwave signal results in a deep modulation of output power level with frequency. Each modulation cycle corresponds to a change in the phase of the output MSSW signal relative to the input signal of 2π. The corresponding change in the MSSW wave number k for a single modulation cycle is $2\pi/\Lambda$, where Λ is the length of the MSSW propagation path.

The fact that the variation in k with frequency shown in Fig. 3(b) has positive slope and is concave upward means that the change in frequency for one modulation period will decrease with frequency. The results in Fig. 4, when expanded in scale, yield a decrease in the modulation period from about 9 MHz near the bottom of the MSSW transmission band up to about 3 MHz at the top of the band.

The level of the modulation may be defined as the peak-to-peak amplitude of the power oscillation divided by the peak power at the very top of a modulation cycle, and multiplied by 100 to yield a percentage modulation factor η. It is clear from the results in Fig. 4(a) that, apart from the initial rapid up and down changes in the modulation near the bottom of the MSSW band, the modulation factor η decreases rapidly as the frequency moves up from the f_o point in Fig. 3(a). This decrease is due to the characteristic increase in the insertion loss with frequency for frequencies above f_o.

The modulation level could be easily controlled by changing the attenuation A in the reference arm of the interferometer. For the minimum insertion loss operating point frequency at

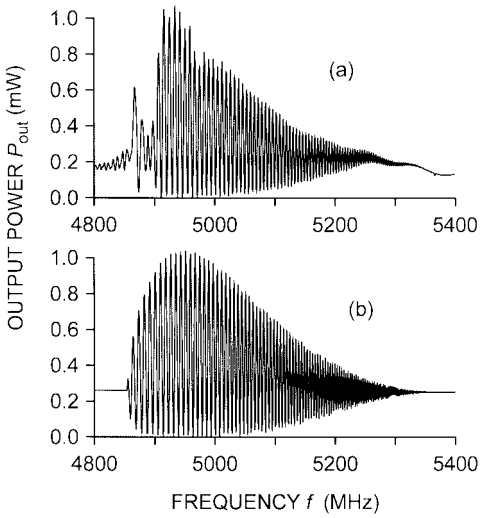

Fig. 4. (a) Measured and (b) calculated frequency responses of the MSSW interferometer without feedback. The input CW power was 1 mW. The operating parameters for the MSSW arm were the same as for Fig. 3. The attenuator setting A for the lower arm of the interferometer in Fig. 2 was -14 dB.

$f_o = 4950$ MHz, for example, an increase in the attenuation A from 0 dB to -14 dB yields a change in η from 60% to 100%. For 5.2 GHz, the same change in A yields a change in η from 15% to 50%.

It is important to note that the overall frequency response of the interferometer in Fig. 4 may be shifted up or down in frequency through an increase or decrease of the magnetic field H, in accordance with the band edge condition of (2). As will be shown shortly, both this field dependence of the interferometer response, and the possibility to control the magnitude of the modulation level of the output, are important considerations for the formation of a bistable device.

Turn now to the details of the calculated interferometer response shown in Fig. 4(b). The equations given here will also be important for the bistability calculations to be considered later. One assumes a CW microwave input signal of frequency f. Based on the various parameters introduced above, along with power divider coefficients of one half for the input divider D and the output combiner C, one may obtain the interferometer power response function $T(k)$ as

$$T(k) = \frac{P_{\text{out}}}{P_{\text{in}}} = \frac{GB}{4}\left[A + L + 2\sqrt{AL}\cos(k\Lambda)\right]. \quad (3)$$

Recall that P_{in} is the power at the input to divider D and P_{out} is the power at the directional coupler take off in Fig. 2. The phase shift of the signal at the MSSW line output was taken to be equal to $k\Lambda$, while the phase shift of the signal in the reference arm channel was taken to be zero. The MSSW wave number k depends on the frequency in accord with the dispersion relation of (1). The MSSW line transmission coefficient L also depends on the frequency. The gain and attenuation factors G, A, and B were taken to be independent on the frequency within the MSSW frequency band. The cosine argument and phase angle $k\Lambda$ will be denoted as θ. This angle will be an important parameter for the analysis of Section IV.

From (1) and (3), in combination with the measured frequency dependence of the MSSW line transmission coefficient L and the values of $P_{\rm in}$, A, B, G, and Λ already cited, one obtains the output power response shown in Fig. 4(b). One can see that the experimental frequency response is matched reasonably well by the theory. The working equations given above reproduce both the decrease in the modulation level and the decrease in the frequency period for the modulation with frequency above the f_o operating point. Note that the actual level of $P_{\rm out}$ depends on the attenuator setting A and the gain coefficient G of the amplifier, so that the $P_{\rm out}/P_{\rm in}$ ratio may be smaller or greater than unity. As with the results in Fig. 3, the notch in the experimental frequency response near 4900 MHz is due to the effect of the substrate metallization on the MSSW dispersion. The additional variations in the experimental power envelope versus frequency in Fig. 4(a) which do not follow the somewhat smoother theoretical result are likely due to uncontrolled reflections in the system which were not taken into account in the modeling.

B. Frequency Response with Feedback

As indicated above, the input microwave power level does not affect the frequency response of the interferometer without external feedback, at least for power levels below 10 dBm or so. The addition of the feedback magnetic field H_F, however, produces a significant change in this frequency response. As one might expect from the feedback arrangement of Fig. 2, higher powers produce bigger effects. The change in the frequency response with power is the basis of the bistable operation to be considered in the next section. This section presents results on the frequency response for increasing powers.

Fig. 5 shows four experimental curves of output power versus frequency. The static field H_S, the amplifier gain G, and the attenuation A were the same as for Fig. 4. There are four differences, however. First, the frequency scale is expanded to show only one modulation cycle or so. These particular data are for frequencies from 4950 to 4962 MHz, close to the operating point frequency f_o for maximum transmission. Second, the four traces are for different values of the input power $P_{\rm in}$. The $P_{\rm in}$ values are -23 dBm for (a), -19 dBm for (b), -15 dBm for (c), and -13 dBm for (d). Third, the data are scaled so that the traces show about the same peak to peak response. The graphs show no vertical numerical scale. The points of comparison concern the change in the shape of the frequency response with power.

The fourth and most important difference between the Figs. 5 and 4 data is that the magnetic field feedback is in place. The Helmholtz coils are connected so that any given level of output power produces an additional magnetic field H_F which subtracts from the static field H_S. The basic effect of higher power, therefore, is to shift the interferometer response to lower frequencies.

The traces in Fig. 5 demonstrate clearly the effect of feedback on the power versus frequency response for a single modulation cycle. Trace (a), for $P_{\rm in} = -23$ dBm, shows that feedback has essentially no effect on the output response when

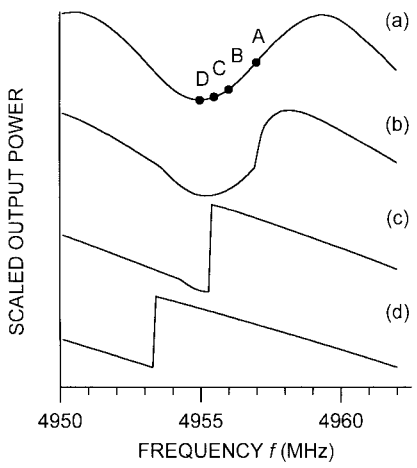

Fig. 5. Measured frequency response curves over a single modulation cycle for the MSSW interferometer with feedback. The feedback magnetic field H_F was configured to subtract from the static magnetic field H_S applied to the MSSW line. The input power $P_{\rm in}$ values for the four traces were (a) -23 dBm, (b) -19 dBm, (c) -15 dBm, and (d) -13 dBm. The other operating parameters for the MSSW arm were the same as for Figs. 3 and 4 and as described in the text. The specific operating points A through D shown on trace (a) are discussed in the text.

the power level is low. Trace (b), for a somewhat higher power at $P_{\rm in} = -19$ dBm, shows a small shift to lower frequency and the development of some distortion in the response from the simple harmonic form in (3) and in trace (a). Traces (c) and (d) show the dramatic effect of higher powers on the response. The increase in $P_{\rm in}$ to -15 dBm, as in trace (c), results in a sawtooth wave response. For these particular system parameters, one has an abrupt jump in output power at about 4955 MHz. When the power is further increased to -13 dBm, as in trace (d), the step frequency shifts down by approximately 2 MHz. This power dependent step response can be used to advantage to achieve bistable operation.

The change in the modulation cycle with power shown in Fig. 5 could be obtained over almost all of the MSSW passband. Empirically, it was found that the precise input power level needed to obtain the sawtooth type response shown in Fig. 5(c) could be reduced in one of two ways, either by decreasing the attenuation A in the fixed arm or by increasing the operating point frequency. Both actions serve to reduce the level of the modulation response.

The distortion in the harmonic interferometer frequency response as the input power is increased, and the sawtooth response which occurs at high powers, may be explained in terms of the feedback effect for different operating frequency points on a given modulation cycle. Four such points are indicated by the labels A, B, C, and D on trace (a) of Fig. 5. These same frequency points will be used as operating points in order to demonstrate bistable power response characteristics in connection with Fig. 6, to be discussed shortly. Note that point D is located at an output power minimum on trace (a). Points C, B, and A are positioned at successively higher power levels and at successively higher frequencies. Note also that the feedback produces a magnetic field H_F which subtracts from the static field H_S. The feedback, therefore, will serve to reduce the net field applied to the MSSW line and shift the

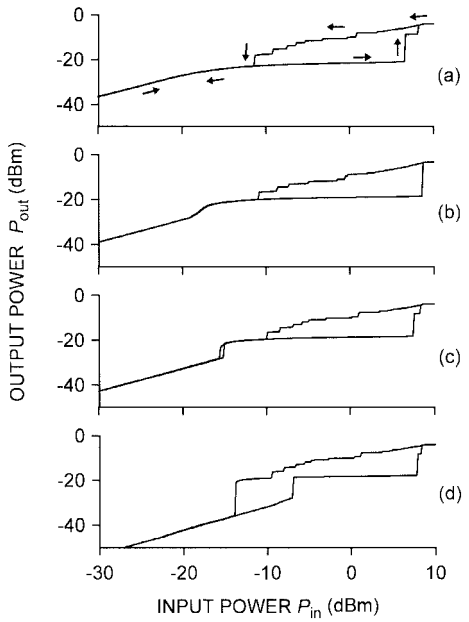

Fig. 6. Typical output power $P_{\rm out}$ versus input power $P_{\rm in}$ response curves for the MSSW bistable interferometer. Curves (a), (b), (c), and (d) correspond to operating point frequencies of 4957 MHz, 4956 MHz, 4955.5 MHz, and 4955 MHz, respectively. The interferometer reference arm attenuator setting was $A = -14$ dB.

overall frequency response shown in Figs. 3 and 4 to lower frequencies.

For point D, the output power is at a minimum point on the modulation cycle in trace (a). Any initial increase in the input power produces only a small increase in H_F and essentially no shift in the overall frequency response. Note that until the sawtooth response is formed for trace (c), the minimum output power frequency position at D in trace (a) remains essentially unchanged at about 4954 MHz.

This situation is maintained for relatively small increases in the input power as one moves up the response curve in trace (a). The portion of trace (b) for frequency points D, C, and B has about the same shape as in trace (a).

However, as the frequency point is moved from point B to point A, the increase in the output power is sufficient to produce a kink in the output power response shown in trace (b). The peak in the output power in trace (b) is now shifted down in frequency to a point just above point A. This is because the feedback field H_F is now increased sufficiently with input power to produce a significant shift in the overall modulation response to lower frequency. As the input power is further increased, the continued increase in H_F causes the kink to shift and accentuate. At some threshold power, as in trace (c), the feedback magnetic field is sufficient to change the simple kink into an abrupt jump in output power, and the overall frequency response is transformed to a sawtooth character. Further increases in power serve simply to shift the sawtooth response to lower frequency.

The response shown in Fig. 5 can be reversed by reversing the sign of the feedback field H_F. In this case, any increase in output power produces a feedback field which adds to the static field H_S and serves to shift the MSSW response curves in Figs. 3 and 4 to higher frequency. In this case, the kink response moves from the low frequency side of the transmission maximum in trace (a) of Fig. 5 to the high frequency side, the kink moves up in frequency as the power is increased. The sawtooth response in trace (c) is also reversed. That is, one obtains a jump in power with decreasing frequency rather than with increasing frequency as in Fig. 5. This jump point will move up in frequency as the power is increased, rather than down in frequency.

C. Bistable Power Response

Fig. 5 showed the response of the system as a function of frequency for different fixed power levels. If the device is operated at fixed frequency and the power is continuously changed, one may obtain the kind of bistable response characteristics which are the objective of this work.

Fig. 6 shows several examples of such a bistable power response. Graphs (a), (b), (c), and (d) in Fig. 6 show curves of output power $P_{\rm out}$ versus input power $P_{\rm in}$ for four different operating point frequencies, as listed in the caption. The sequence of graphs from (a) to (d) correspond to frequency operating points which match the frequency points labeled from A to D in Fig. 5(a). These data were all obtained for a reference arm attenuator setting $A = -14$ dB and with the feedback magnetic field H_F configured to subtract from the static field H_S. All other operating parameters were the same as established above. The cycle time for the measurement of one power cycle was 30 s. The arrows in (a) indicate directions of power changes along the individual portions of the cycle, as will be discussed below. Arrows are not shown on the other diagrams.

Fig. 6(a) corresponds to an operating point frequency of 4957 MHz, the same as point A in Fig. 5(a). The data in Fig. 6(a) show that as the input power is initially increased from a low value of -30 dBm, the output power increases somewhat and then saturates at about -22 dBm. As indicated by the arrows, this leg of the cycle is entirely reversible as long as $P_{\rm in}$ does not exceed about $+7$ dBm. If the input power is increased above $+7$ dBm, there is an abrupt jump in the output power from -22 dBm to about -4 dBm, and a further gradual increase as $P_{\rm in}$ approaches the $+10$ dBm limit for nonlinear effects. As $P_{\rm in}$ is then decreased, the $P_{\rm out}$ level only drops slowly, does not retrace the previous jump at $P_{\rm in} \approx +7$ dBm, and finally rejoins the initial response curve at $P_{\rm in} \approx -11$ to -12 dBm or so. This return path is indicated by the arrows beside the top response curve. There are also several smaller jumps which decorate this $P_{\rm out}$ versus $P_{\rm in}$ response curve cycle.

The data in Fig. 6(a) demonstrate clearly the hysteretic nature of the $P_{\rm out}$ versus $P_{\rm in}$ response for the MSSW interferometer with magnetic field feedback. This response corresponds, moreover, to a bistable output. For an input power in the range -12 dBm $< P_{\rm in} < +7$ dBm, one has two different possible values of $P_{\rm out}$. This is precisely the transmission characteristic which is typical for a bistable system of the sort shown in Fig. 1. The presence of numerous minor jumps on the overall bistable response curve provides further signatures of system bistability.

The remaining power response curves in Fig. 6 show the change in the bistable response characteristics which result for different operating point frequencies. Graphs (b), (c), and (d) correspond to operating point frequencies of 4956 MHz, 4955.5 MHz, and 4955 MHz, respectively, the same as the B, C, and D frequency points indicated in Fig. 5(a). The effect of these changes in frequency is to develop a second bistable region for lower input power levels which opens up abruptly and merges with the main bistable power hysteresis loop.

The beginnings of this second region are evident in Fig. 6(b) by the small region near $P_{\rm in} = -18$ dBm with an increased slope. As the operating point frequency moves lower, to point C in Fig. 5(a), this small region of increased slope first opens up slightly, as in Fig. 6(c). As the operating point frequency moves to the bottom of the Fig. 5(a) response curve at point D, the new part of the bistable response opens up completely and merges with the initial bistable response. This result is shown in Fig. 6(d).

A further decrease in the operating point frequency shifts the operating point into the Fig. 5(a) response region to the left of point D. This shift initially results in a further broadening of the second hysteresis loop. As the operating point continues to move down in frequency and up the response curve of Fig. 5(a), one observes a smooth transition back to a bistable response of the sort in Fig. 6(a) and the cycle then repeats.

The bistable character demonstrated above is a result of the interferometer response in combination with magnetic field feedback derived from that response. The amount of the realized bistability for a given operating point frequency can be controlled through a change in the attenuation in the lower arm of the interferometer. A decrease in the attenuation, for example, will serve to reduce the level of modulation and the modulation factor η defined above. This, in turn, will reduce the level of the overall bistable response with feedback in place.

This effect is demonstrated in Fig. 7. Bistable power response curves are shown in the same format as in Fig. 6. For these data, however, the operating point frequency was held constant at 4957 MHz, just at point A in Fig. 5(a), and the level of the attenuation in the reference arm of the MSSW interferometer was changed. Graphs (a), (b), (c), and (d) are for values of the attenuation A in Fig. 2 of -14 dB, -10 dB, -5 dB, and zero dB, respectively. Without feedback, the modulation factor η ranged from 100% at $A = -14$ dB to 60% at $A = 0$ dB.

The response curves in Fig. 7 show that a decrease in the attenuation, and the corresponding decrease in the modulation, leads to three effects. First, there is a shift in the bistable power response curve as a whole to lower input power values. Second, the power hysteresis loop becomes narrower. Three, there appears a large number of small jumps in the output power for both the increasing input power and decreasing input power legs of the cycle.

One would expect that the range of input power values over which the bistable response takes place could be shifted by a change in the amount of feedback. For the set up used here, it was found that a decrease in the dc current amplifier gain by a factor of 10 or the introduction of an additional -10 dB of attenuation in the feedback loop just before the detector in Fig. 2 resulted in a shift in the bistable response characteristic as a whole by about of 10 dB to higher input power levels.

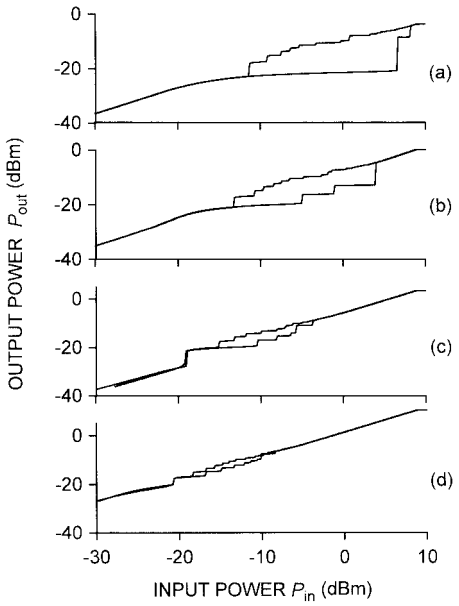

Fig. 7. Typical output power $P_{\rm out}$ versus input power $P_{\rm in}$ response curves for the MSSW bistable interferometer. Curves (a), (b), (c), and (d) correspond to interferometer reference arm attenuator settings of -14 dB, -10 dB, -5 dB, and zero dB, respectively. The operating point frequency was 4957 MHz.

In summary, the data of Figs. 6 and 7 clearly show that the MSSW interferometer with external feedback can be used to produce a bistable or multistable output versus input power response. The character of the response can be controlled through the choice of the operating point frequency position relative to an individual interferometer response without feedback. The level of the bistable or multistable response can be controlled by the attenuation in the reference arm of the interferometer. The position of the response can be controlled by the level of the feedback response.

D. Bistable Power Response for Pulsed Experiments

The abrupt jumps in output power which produce the bistable response profiles in Figs. 6 and 7 were obtained during automatic input power scans controlled by the microwave transition analyzer (MTA) unit in Fig. 2. The MTA unit, when operated in a power scan mode, works in the same way as a sampling oscilloscope. The unit cycles $P_{\rm in}$ up and then down through the specified input power range over and over. During each cycle, the sample time is incremented in such a way as to obtain response curves shown in Figs. 6 and 7. Implicit in this procedure is a sample time per step. Based on the MTA set up for the measurements shown, the abrupt up and down jumps in Figs. 6 and 7 occurred over times which were below about 120 ms.

If the bistable microwave response presented above is to be useful for radar applications, whatever actual device is developed will most likely be operated in a pulsed mode. The chief drawback of the demonstration system described here is in the large time constant for any change in the feedback

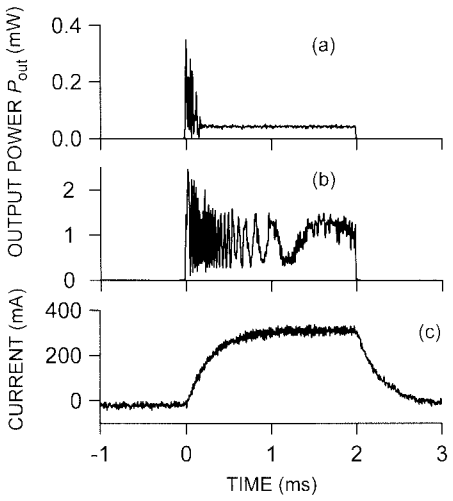

Fig. 8. Graphs (a) and (b) show output power $P_{\rm out}$ versus time responses to 2 ms wide input pulses at the input power $P_{\rm in}$ values indicated. The input pulse commenced at time zero on the scale of the graphs. The input pulse carrier frequency was 4950 MHz. The reference arm attenuator setting was -14 dB. Other experimental parameters were the same as for previous figures and given in the text. Graph (c) shows the time dependence of the current which drives the Helmholtz coils used to provide the feedback magnetic field.

magnetic field produced by the Helmholtz coil. Measurements in a pulsed mode of operation have been made to demonstrate that the response time limitation for bistability is due to the Helmholtz coil. If faster rise time fields can be produced, the response time for bistable operation will be limited only by the relaxation time of the MSSN signal. This time is typically in the 100 ns range.

These pulse measurements were made with 2 ms wide microwave pulses of rectangular shape with a rise time of less than 0.1 μs and a peak power up to $P_{\rm in} = 20$ dBm. These pulses were formed by a internal modulator which is part of the MTA unit. The operating point carrier frequency of the pulses was set at 4950 MHz. The reference arm attenuation was set at -14 dB and the feedback magnetic field was connected to produced a shift of the interferometer frequency response curve to lower frequencies.

Fig. 8 shows three time traces. Graphs (a) and (b) show output power versus time for a low $P_{\rm in}$ value of -1 dBm and a relatively high $P_{\rm in}$ value of $+9$ dBm, respectively. Graph (c) shows the time dependence of the feedback current applied to the Helmholtz coil which corresponds to the power response of graph (b). The leading edge of the input microwave pulse signal occurs at time zero on the scale of Fig. 8.

For input peak powers below about -10 dBm, the output pulse response strictly reproduced the rectangular shape of the input signal. Above -10 dBm, one observes modulation effects at the beginning of the pulse for relatively low powers and extending over the entire pulse for high powers. Graph (a) is typical of the output power response for relatively low input peak power levels above the -10 dBm threshold. Here, one finds a periodic modulation at the very beginning of the pulse, followed by a constant power output to the end of the pulse. This type of response is clearly related to the rapid rise in the input signal. It occurs too fast to be related to the feedback magnetic field response shown by the current response in graph (c).

At the high end of the range of available powers, one obtains the type of response shown in graph (b). Here, the output power exhibits a rapid oscillation during the rise time of the feedback current and magnetic field. The amplitude of this oscillation decreases with time and the period increases. Note that the Helmholtz coil inductance limited response time of the feedback shown in graph (c) was about 0.3 ms. The oscillation response clearly tracks this feedback. The decrease in amplitude of the oscillation is due to the down shift in the MSSW frequency response as the feedback field grows and the corresponding increase in the MSSW insertion loss. The increase in the period of the oscillation is due to the gradual leveling off of the feedback current and field.

The data in Fig. 8 demonstrate that the frequency shifts and power response which leads to bistability are dominated by the response time of the feedback magnetic field. There are ways in which this response time could be reduced. One could, for example, use a broadband high current dc amplifier in combination with low inductance coils or a microstrip transmission line to produce the feedback field [1]. A feedback field response up to about 100 Oe/μs could be achieved in this way. In this limit, the characteristic time of the bistable system will be determined by the MSSW response time. This time could be well below 1 μs, depending on the operating point and MSSW parameters.

IV. Bistable Response Analysis

A. Load Line Analysis of the Bistable Response

An understanding of the bistable response of the MSSW interferometer presented above can be obtained from a graphical approach similar to that used in [11] for nonlinear optical resonators. For the MSSW interferometer, one starts with the interferometer response function of (3) for $T(k)$. It is important to keep in mind that (3) describes the interferometer response alone, with no explicit consideration of feedback.

In the presence of feedback, one must take into account a second condition on $T(k)$, based on the fact that the interferometer output results in an additional magnetic field which, under constant frequency conditions, will serve to shift the MSSW wave number. This shift may be expressed as

$$k = k_o + \beta P_{\rm out} \tag{4}$$

where k is the shifted wave number, k_o is the operating point wave number in the limit of very low powers, and β is a feedback coefficient. The size of the parameter β is controlled by the detector, the amplifier, and the field-current calibration of the Helmholtz coil which define the feedback part of the circuit in Fig. 2, as well as the MSSW operating point itself. The sign of β is determined by the manner in which the feedback is connected. If the feedback magnetic field is opposite to the static magnetic field, the feedback will cause the wave number k to increase under constant frequency conditions and β would be positive. Values of k_o and β appropriate for the experimental set up and operating point conditions for the previous section are 127 rad/cm and 700 rad $\cdot$ mW/cm, respectively.

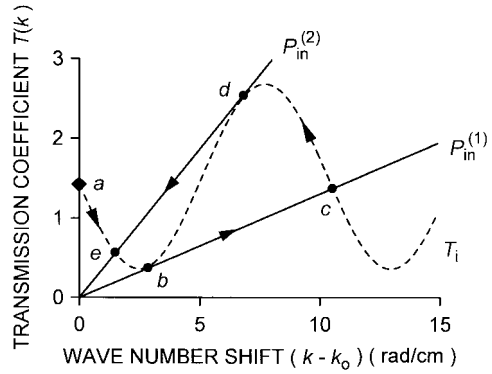

Fig. 9. Response functions for the transmission coefficient T as a function of wave number k for the MSSW interferometer with feedback. Wave number is shown as the shift from the operating point wave number k_o in the absence of any feedback magnetic field. The dashed curve shows the MSSW interferometer response from (3). The straight solid lines represent load lines for T versus $(k - k_o)$ for two different critical input power levels $P_{\rm in}^{(1)}$ and $P_{\rm in}^{(2)}$ as described in the text. The MSSW operating point and other system parameters on which the plots are based are given in the text, as is the significance of the labeled points and arrows.

From (4), one may readily obtain the second condition on $T(k)$. This condition is given by

$$T(k) = \frac{P_{\rm out}}{P_{\rm in}} = \frac{k - k_o}{\beta P_{\rm in}}. \tag{5}$$

For a given input power level, and with feedback in place, $P_{\rm out}$ must be such that both (3) and (5) are satisfied. The k dependence of T in (3) is oscillatory. The k dependence of T in (5) is linear, and the slope of the response is inversely proportional to $P_{\rm in}$. Equation (5) provides a load line of sorts with which to select out valid operating points on the oscillatory response from (3). The interplay of these two dependences provide a direct way to understand multistability for the MSSW interferometer with feedback.

Fig. 9 shows representative plots of $T(k)$ as a function of the wave number shift $(k-k_o)$ from (3) and (5) for the k_o and β values given above, and an attenuation $A = -7$ dB. The other relevant experimental parameters as the same given in previous sections. The two solid lines labeled $P_{\rm in}^{(1)}$ and $P_{\rm in}^{(2)}$ illustrate the $T(k)$ constraint from (5) for two different input power levels. The significance of these lines will be considered shortly. The dashed T_i curve represents (3). This sinusoidal curve is just the interferometer response considered in the previous section. The maxima on the sinusoid correspond to $k\Lambda$ phase angles which are an integer multiple of 2π. The minima correspond to phase angles which are an odd integer multiple of π.

In order to understand the bistable response characteristic from Fig. 9, consider first the situation for very low input power levels. In this limit of very low $P_{\rm in}$ values, the load line represented by (5) will be nearly vertical, and point a in Fig. 9, indicated by the filled diamond symbol, will mark the intersection point of this line and the dashed T_i curve. This intersection determines the transmission coefficient T and the $P_{\rm out}/P_{\rm in}$ ratio in the very low power limit.

As the input power is increased, the slope of the load line will decrease, and, as indicated by the arrow, one will begin to move down the T_i curve in a smooth and reversible manner. This behavior will continue until the input power is sufficient to reach point b. The $P_{\rm in}^{(1)}$ line and point b represent the highest input power for a smooth, continuous, and reversible output power versus input power response from the lowest power levels.

As soon as the input power reaches $P_{\rm in}^{(1)}$, there will be a discontinuous jump in the T coefficient from point b to point c. This jump is indicated by the arrow on the b-c segment of the $P_{\rm in}^{(1)}$ line. Note that for the same input power, point c corresponds to a large jump in output power. From point c, now consider the effect of reducing the input power. One would now follow the T_i curve from point c in the direction of increasing T values as indicated by the arrow, until point d is reached. At this point, the reverse of the jump process just described would occur and there would be a jump back to point e on the a-b segment of the T_i curve. This jump is indicated by the arrow on the d-e segment of the $P_{\rm in}^{(2)}$ line.

The e-b and the c-d segments of the T_i interferometer response curve constitute one bistable region for the $P_{\rm out}$ versus $P_{\rm in}$ response. These segments are sandwiched between two specific input power dependent load lines, $P_{\rm in}^{(1)}$ and $P_{\rm in}^{(2)}$. These two power levels and the corresponding load line segments constitute the jump points for the bistable response.

The process depicted in Fig. 9 may also lead to a multistable response as well. One could, for example, continue to increase $P_{\rm in}$ after the initial jump from b to c. In this case, the operating point on the T_i curve would continue to move to the right until the next jump point is reached close to the bottom of the second minimum region on the curve near $(k - k_o) \approx 13$ rad/cm. If one continued to increase $P_{\rm in}$, this process would be repeated cycle by cycle. A similar scenario takes place when $P_{\rm in}$ is decreased from some high value. In this case, the jumps occur near the maximum points on the T_i curve, as from points d to e in Fig. 9, and serve to decrease T when the jump occurs.

B. Calculated Bistable Response

Explicit bistable and multistable response curves of $P_{\rm out}$ versus $P_{\rm in}$ for the MSSW interferometer can be evaluated numerically. Such evaluations are based on the load line and interferometer response considerations given above, the MSSW wave number versus frequency characteristic given in (1), and the actual $H_F(P_{\rm out})$ response of the feedback circuit. The results presented below are based on an empirical determination of $H_F(P_{\rm out})$ obtained as

$$H_F(P_{\rm out}) = \begin{cases} 95\left(1 - e^{-2P_{\rm out}[\rm mW]}\right)[\rm Oe], & P_{\rm out} < 0.4 \text{ mW} \\ 52.5 \text{ Oe}, & P_{\rm out} \geq 0.4 \text{ mW}. \end{cases} \tag{6}$$

The $H_F(P_{\rm out})$ response of (6) has an accuracy of a few percent, with $P_{\rm out}$ values specified in mW and H_F values obtained in Oe.

With H_F now known for a given $P_{\rm out}$ value, (1) yields the shift in the wave number k from the value k_o at $H_F = 0$ for a given operating point frequency and static field. Based on the above, one now has the wave number k as a function of $P_{\rm out}$. One may now evaluate $P_{\rm in}$ as a function of $P_{\rm out}$ from

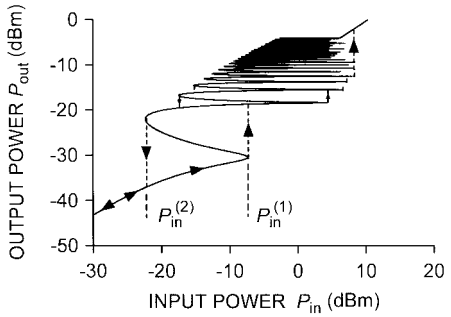

Fig. 10. Computed $P_{\rm in} - P_{\rm out}$ response function for the MSS winterferometer with feedback. The operating point frequency was taken to be 4955 MHz and the interferometer reference arm attenuation A was taken as -12.5 dB. Other parameters were the same as for the experiment. The dashed lines and arrows show jumps which would correspond to the measured bistable or multistable response for the experiment. The $P_{\rm in}^{(1)}$ and $P_{\rm in}^{(2)}$ labels indicate the power levels for the two major jumps from the low-to-high and the high-to-low power states, respectively.

a variation of (3)

$$P_{\rm in} = \frac{4P_{\rm out}}{GB[A + L(k) + 2\sqrt{AL(k)}\cos(k\Lambda)]}. \qquad (7)$$

The dependence of the MSSW line transmission loss on the wave number, specified explicitly in (7) as $L(k)$, is calculated numerically by the method given in [8], as in Section II-A above. Once this is done, one may plot $P_{\rm in}$ on the horizontal axis and $P_{\rm out}$ on the vertical axis to obtain the response function which generates bistable and multistable behavior.

Such a $P_{\rm in} - P_{\rm out}$ response function plot is shown by the solid curve in Fig. 10. This curve was obtained for an attenuation $A = -12.6$ dB and a frequency $f = 4955$ MHz. All other parameters are the same as given previously. Note that the parameters chosen for this evaluation are close to those which apply to Fig. 6(d). The dashed lines, arrows, and other labels are intended to designate various peculiarities of the response function which lead to bistability. These features will be considered shortly.

Recall from the mechanics of the calculation that the response is obtained as a functional dependence of $P_{\rm in}$ on $P_{\rm out}$. Viewed in this way, it is seen that the response curve consists of many peaks, some pointing to the right and some pointing to the left on a $P_{\rm out}$ versus $P_{\rm in}$ plot of the sort shown in Fig. 10. With $P_{\rm in}$ as the control parameter for an experiment, the practical effect of this response curve is to produce jumps in $P_{\rm out}$. These jumps will be in the direction of larger output power levels at the point(s) for which $P_{\rm in}$ is increasing and reaches an extremum which points to the right. One such jump occurs at the upward pointing vertical arrow labeled $P_{\rm in}^{(1)}$. The jumps will be in the direction of smaller output power levels at the point(s) for which $P_{\rm in}$ is decreasing and reaches an extremum which points to the left. A jump of this sort occurs at the downward pointing vertical arrow labeled in $P_{\rm in}^{(2)}$ Fig. 10.

The jumps at $P_{\rm in}^{(1)}$ and $P_{\rm in}^{(2)}$ are associated with the two extrema on the response curve in Fig. 10 with the biggest separation in $P_{\rm out}$ values. As the figure shows, the total response curve consists of many right and left pointing extrema, some of which are rather closely spaced. These extrema give rise to small sequential jumps in $P_{\rm out}$ of the sort which decorate the bistable response data of Figs. 6 and 7. If one were to take all the jumps which would occur at all of the extrema shown in Fig. 10, these jumps and the continuous response regions in between would form a bistable $P_{\rm out}$ versus $P_{\rm in}$ curve very similar to the one shown in Fig. 6(d), for example.

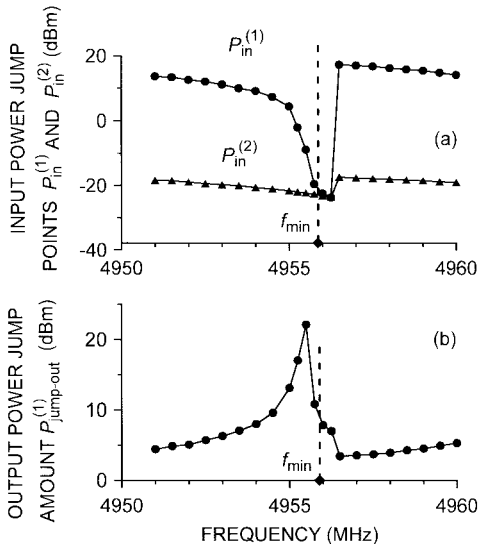

Fig. 11. Graph (a) shows the change in the values of the input power at the $P_{\rm in}^{(1)}$ and $P_{\rm in}^{(2)}$ jump points in Fig. 10 with operating point frequency. Graph (b) shows the amount of the jump in $P_{\rm out}$ at the $P_{\rm in}^{(1)}$ jump point, $P_{\rm jump\_out}^{(1)}$, versus the operating point frequency. All results are based on computed curves of the sort shown in Fig. 10. The vertical dashed line denoted by $f_{\rm min}$ indicates the frequency at the point of a minimum in the output power with no feedback which corresponds to point D in Fig. 5.

The computed response in Fig. 10 demonstrates the origin of a bistable response for the MSSW interferometer with feedback. Additional computations were used to explore more systematically the effect of frequency on the bistable response. The main bistable response parameters are (a) the spacing in input power between the jump points $P_{\rm in}^{(1)}$ and $P_{\rm in}^{(2)}$, and (b) the size of the jumps in $P_{\rm out}$ at $P_{\rm in}^{(1)}$ and $P_{\rm in}^{(2)}$. Some selected results are shown in Fig. 11. Graph (a) shows the effect of different operating point frequencies on the position of the high power jump point $P_{\rm in}^{(1)}$ for an increase in $P_{\rm out}$ and on the position of the high power jump point $P_{\rm in}^{(2)}$ for a decrease in $P_{\rm out}$. Graph (b) shows the amount of the jump in $P_{\rm out}$ at $P_{\rm in}^{(1)}$, denoted as $P_{\rm jump\text{-}out}^{(1)}$, with frequency. The vertical dashed line at $f_{\rm min}$ shows the frequency point for minimum output power in the case of no feedback, as at point D in Fig. 5(a). The range of frequency values examined in Fig. 11 correspond to one full cycle for the response without feedback shown in Fig. 5.

One can see from Fig. 11(a) that the jump point $P_{\rm in}^{(1)}$ exceeds the jump point $P_{\rm in}^{(2)}$ by about 30–35 dB when the signal frequency is far below the minimum transmission point at $f_{\rm min}$. As the operating point frequency approaches $f_{\rm min}$, the $P_{\rm in}^{(1)}$ jump point decreases rapidly and produces a severe narrowing in power of the bistable loop. If the frequency is increased further, the loop widens abruptly back to 35–40 dB or so after a frequency change of only 1 MHz or so. This completes one response cycle.

Fig. 11(a) shows a continuous narrowing in the width of the bistable response hysteresis loop as one approaches the $f_{\min}$ point from lower frequencies, due to the $P_{\text{in}}^{(1)}$ change with frequency just discussed. In contrast, Fig. 11(b) shows that the height of the bistable response increases to a sharp maximum which exceeds 20 dB at a frequency just below $f_{\min}$. The combined effect of these two responses is the achievement of the largest overall bistable response, in terms of both width and height, at some select frequency operating point just below $f_{\min}$.

The numerical analysis also showed that the main effect of a change in frequency is on the width and height of the major parts of the bistable response. Changes in frequency had little effect on the higher order steps evident from Fig. 10 and from the data in Figs. 6 and 7. This result is consistent with the response scenario discussed in connection with Fig. 9. At very high powers, the straight line response constraint will have a very small slope and will lead to jump points which derive from higher order response cycles well to the right of the cycle shown. These higher order jump points will be relatively insensitive to the precise frequency of operation.

Calculations of P_{out} versus P_{in} curves of the sort shown in Fig. 10 were also done for values of the attenuation A from 0 to -14 dB. The results showed a clear narrowing in the bistable response, in agreement with the observed narrowing shown in Fig. 7.

C. Operational Considerations

The results shown in Figs. 10 and 11 are representative of the load line model given in Section IV-A. The detailed bistable response characteristics of a given MSW device will depend, of course, on the explicit parameters of the set up, the feedback response, etc., and should be calculated for each specific case. However, the simple load line model of (3)–(5) and Fig. 9 allows one to make several observations which are of general applicability.

Consider the dashed line sinusoidal interferometer transmission response curve in Fig. 9 for $T(k)$, based on (3), and the position of the $P_{\text{in}}^{(1)}$ load line. It is clear from Fig. 9 that the jump point b is generally positioned on the dashed line sinusoid at a point which is close to the first minimum. This minimum point corresponds to a value of the $k\Lambda$, the wave number-transducer separation product, which is some odd integer multiple of π. To a good approximation, therefore, the $T(k)$ condition at point b from (4) may be written as

$$\frac{P_{\text{out}}^{(b)}}{P_{\text{in}}^{(1)}} = \frac{GB}{4}\left[A + L - 2\sqrt{AL}\right] \tag{8}$$

where $P_{\text{out}}^{(b)}$ is the output power at point b.

Similar considerations may be applied to point c. From the topology of the interferometer response sinusoid and the $P_{\text{in}}^{(1)}$ load line, it is clear that the change in the $k\Lambda$ phase angle from point b to point c will be between π and 2π. This change in phase angle will be denoted as θ_{bc}. The $T(k)$ condition at point c may now be written as

$$\frac{P_{\text{out}}^{(c)}}{P_{\text{in}}^{(1)}} = \frac{GB}{4}\left[A + L - 2\sqrt{AL}\cos(\theta_{bc})\right] \tag{9}$$

where $P_{\text{out}}^{(c)}$ is the output power at point c.

Equation (5) yields one final result for this analysis. Note that the phase angle θ_{bc} is simply equal to the change in the $k\Lambda$ product from point b to point c. Equation (5), therefore, yields a simple expression for $(P_{\text{out}}^{(c)} - P_{\text{out}}^{(b)}) = P_{\text{jump-out}}^{(1)}$

$$P_{\text{out}}^{(c)} - P_{\text{out}}^{(b)} = P_{\text{jump-out}}^{(1)} = \frac{\theta_{bc}}{\Lambda\beta}. \tag{10}$$

Recall that $P_{\text{jump-out}}^{(1)}$ is the jump in output power at input power $P_{\text{in}}^{(1)}$ considered in Fig. 11(b). Equation (10) provides an immediate indication of the considerations needed to optimize the size of the bistable jump in output power. The jump in power will be largest when both the MSSW propagation path length Λ and the feedback field response coefficient β are small. It is clear from the previous discussions, however, that the feedback field is the cause of the bistability in the first place. The feedback produces the bistability. The above result shows that more and more feedback also serves to diminish the size of the bistable jump.

Equations (8)–(10) may be readily solved for $P_{\text{in}}^{(1)}$. The result is

$$P_{\text{in}}^{(1)} = \frac{\theta_{bc}}{\Lambda\beta}\frac{4}{GB}\frac{1}{2\sqrt{AL}[1-\cos(\theta_{bc})]}. \tag{11}$$

The first factor on the right-hand side of (11) is just the $P_{\text{jump-out}}^{(1)}$ expression from (10). The various parameters of the MSSW circuit all enter in the denominator. An increase in any of these parameters, therefore, can serve to push the input power jump point to lower values. One could perform a similar analysis for the jump from d to e and obtain very similar equations for $P_{\text{jump-out}}^{(2)}$ and $P_{\text{in}}^{(2)}$. It is clear that a wide range of bistable response regimes are possible.

V. Comment on Applications

The above results deal exclusively with the microwave magnetic considerations and principles of operation of an MSW based bistable microwave power device. From the nature of the specific feedback and the results of Fig. 8, it is clear that the device in its present form would be useful only for slow speed applications. The use of Helmholtz coils to provide the feedback magnetic field gives a response time limitation of a millisecond or so. It is likely that fast response times will be an important consideration for device applications. A relatively fast bistable MSW device, for example, would open the possibility to switch rapidly the level of a given microwave signal between two different steady state values simply by applying an additional input pulse of the right power. Such a device could form the basis for microwave power logic.

Two alternative feedback approaches might be considered. One approach would be to use feedback to modify the operating temperature in some way. The temperature dependence of the ferrite magnetization and anisotropy field is known to

bring about a shift in the ferromagnetic resonance [12]. This shift would also occur for MSW signals and could lead to a bistable response of the same sort as documented above. Such a thermally driven mechanism might also have response time limitations, although this is not a foregone conclusion for thin films.

The second approach could involve the nonlinear response of the ferrite film. A frequency shift of MSW signals due to the intrinsic nonlinear response of the system has been observed experimentally [13]. These processes, if they could be used as a means for feedback, could be used to design a simple bistable MSW device. The response time limitation in this case would be on the order of the spin wave relaxation time, which is typically in the 100 nanosecond range.

VI. Summary

Microwave bistability and multistability in a hybrid magnetostatic spin wave interferometer have been observed and investigated. The interferometer contained an MSSW transmission line, an attenuator in the reference channel, and a feedback signal in the form of an additional static magnetic field applied to the MSSW line. This feedback field was driven by the power response of the MSSW interferometer. Feedback resulted in a dramatic nonlinear distortion of the interferometer frequency response and gave rise to an appearance of typical bistable or multistable response characteristics for output power versus input power at constant frequency. Possibilities to control the bistable response by changing the frequency of microwave signal, the attenuation in the reference channel, and sensitivity of the feedback loop were demonstrated experimentally and confirmed theoretically. A simple method for the calculation of these bistable response characteristics was also developed. Both the data and the theoretical response analysis show various ways to control the bistable response.

Appendix
Definitions of Symbols and Acronyms

MSW	Magnetostatic wave.
YIG	Yttrium iron garnet.
P_{out}	Output power.
P_{in}	Input power.
$P_{\text{in}}^{(1)}$	Input power at the bistable jump point for an increase in output power.
$P_{\text{in}}^{(2)}$	Input power at the bistable jump point for a decrease in output power.
MSSW	Magnetostatic surface wave.
A	Attenuation in reference arm of MSSW interferometer.
H	Total magnetic field applied to MSSW device.
L	MSSW line power transmission coefficient.
D	Power divider at input to MSSW interferometer.
C	Power combiner at output from MSSW interferometer.
G	Gain of microwave amplifier after MSSW interferometer.
Λ	Separation of input and output microstrip transducers for the YIG film MSSW transmission line.
H_S	Static external magnetic field applied to MSSW device.
H_F	Feedback magnetic field applied to MSSW device.
E	Directional coupler to sample output power from overall device.
P_d	Microwave power at diode input point in feedback loop.
k	Magnetostatic wave wave number.
f	Magnetostatic wave frequency.
$\|\gamma\|$	Absolute value of the gyromagnetic ratio.
f_H	Frequency parameter for the static magnetic field defined by $f_H = \|\gamma\|H$.
$4\pi M$	Saturation induction.
f_M	Frequency parameter for the saturation induction defined by $f_M = \|\gamma\|4\pi M$.
f_B	Low frequency MSSW band edge defined by $f_B = \sqrt{f_H(f_H + f_M)}$.
f_o	Operating point carrier frequency.
η	Percentage modulation factor.
$T(k)$	Interferometer power transmission coefficient.
θ	Phase angle defined by $\theta = \Lambda k$.
k_o	Operating point wave number in limit of low power.
β	Feedback coefficient.
T_i	Interferometer response curve without feedback.
$P_{\text{jump-out}}^{(1)}$	Size of jump in output power at the input power jump point $P_{\text{in}}^{(1)}$.
$f_{\min}$	Frequency for minimum transmission coefficient without feedback.
$P_{\text{out}}^{(b)}$	Output power at the start of the jump in output power at point b in Fig. 9.
θ_{bc}	Change in the phase angle θ during the jump in output power from point b to point c in Fig. 9.
$P_{\text{out}}^{(c)}$	Output power at the end of the jump in output power at point c in Fig. 9.

Acknowledgment

The YIG film sample was provided by Dr. J. D. Adam of the Northrop Grumman Research and Development Laboratories, Pittsburgh, PA. The authors would like to thank M. M. Scott for a careful reading of the manuscript.

References

[1] Y. K. Fetisov, "Propagation and interaction of magnetostatic spin waves in planar magnetic structures with nonstationary parameters," *High Frequency Processes in Magnetic Materials*, G. Srinivasan and A. N. Slavin, Eds. Singapore: World Scientific, 1995, pp. 203–249.

[2] Y. K. Fetisov, "Microwave signal processing using magnetostatic waves in planar ferrite structures with nonstationary parameters," in *Proc. 1994 Asia Pacific Microwave Conf.*, Tokyo, Japan, Dec. 6–9, 1994, vol. 1, pp. 167–170.

[3] H. M. Gibbs, *Optical Bistability: Controlling Light with Light.* New York: Academic, 1985.

[4] A. D. Boardman, S. A. Nikitov, and Q. Wang, "Theory of bistable magnetostatic surface waves," *IEEE Trans. Magn.*, vol. 30, pp. 1–13, Jan. 1994.
[5] Y. K. Fetisov, P. Kabos, and C. E. Patton, "Bistable microwave oscillator with magnetostatic wave signal-to-noise enhancer in the feedback loop," *Electr. Lett.*, vol. 32, no. 20, pp. 1894–1895, Sept. 1996.
[6] J. D. Adam, M. R. Daniel, P. R. Emtage, and S. H. Talisa, "Magnetostatic waves," *Physics of Thin Films. Advances in Research and Developments, Thin Films for Advanced Electronics Devices*, M. H. Francombe and J. H. Vossen, Eds. Boston, MA: Academic, 1991, vol. 15, pp. 1–141.
[7] R. W. Damon and J. H. Eshbach, "Magnetostatic modes of a ferromagnetic slab," *J. Phys. Chem. Solids*, vol. 19, no. 3/4, pp. 308–320, 1961.
[8] G. A. Vugalter and V. N. Makhalin, "Reflection and excitation of surface magnetostatic waves by a metal strip," *Sov. Phys. Tech. Phys.*, vol. 30, pp. 296–300, 1985.
[9] W. Shiltz, "Spin-wave propagation in epitaxial YIG films," *Philips Res. Rep.*, vol. 28, no. 1, pp. 50–61, 1973.
[10] W. L. Bongianni, "Magnetostatic propagation in a dielectric layered structure," *J. Appl. Phys.*, vol. 43, pp. 2541–2548, 1972.
[11] F. S. Felber and J. H. Marburger, "Theory of nonresonant multistable optical devices," *Appl. Phys. Lett.*, vol. 28, pp. 731–734, 1976.
[12] K. D. McKinstry, C. E. Patton, and M. Kogekar, "Low power nonlinear effects in the ferromagnetic resonance of yttrium iron garnet," *J. Appl. Phys.*, vol. 58, no. 2, pp. 925–929, July 1985.
[13] M. A. Tsankov, M. Chen, and C. E. Patton, "Magnetostatic wave dynamic magnetization response in yttrium iron garnet films," *J. Appl. Phys.*, vol. 79, no. 3, pp. 1595–1603, Feb. 1996.